The Mediterranean Ocean Colour Level 3 Operational Multi-Sensor Processing

Gianluca Volpe[1], Simone Colella[1], Vittorio Brando[1], Vega Forneris[1], Flavio La Padula[1], Annalisa Di Cicco[1], Michela Sammartino[1], Marco Bracaglia[1,2], Florinda Artuso[3], Rosalia Santoleri[1]

[1] Istituto di Scienze dell'Atmosfera e del Clima, Via Fosso del Cavaliere 100, 00133, Roma, Italy
[2] Università degli Studi di Napoli Parthenope,Via Amm. F. Acton 38, 80133, Naples, Italy
[3] Ente per le Nuove tecnologie l'Energia e l'Ambiente, Dipartimento Ambiente, Centro Ricerche Frascati, Frascati, Italy

Correspondence to: Gianluca Volpe (gianluca.volpe@cnr.it)

Abstract. This work describes the main processing steps operationally performed to enable single ocean colour sensors to enter the multi-sensor chain for the Mediterranean Sea of Ocean Colour Thematic Assembling Centre. Here, the multi-sensor chain takes care of reducing the inter-sensor bias before data from different sensors are merged together. The basin-scale in situ bio-optical dataset is used both to fine-tuning the algorithms for the retrieval of phytoplankton chlorophyll and attenuation coefficient of light, Kd, and to assess the uncertainty associated with them. The satellite multi-sensor remote sensing Reflectance spectra better agree with the in situ observations than that of the single sensors, and are comparable with the ESA-OC-CCI multi-sensor product, highlighting the importance of reducing the inter-sensor bias. The Mediterranean near-real-time multi-sensor processing chain has been set up and is operational in the framework of the Copernicus Marine Environment Monitoring Service.

Introduction

The Copernicus Marine Environment Monitoring Service (CMEMS) is one of the six services of the Copernicus program. It provides regular and systematic reference information on the physical state, variability and dynamics of the ocean, ice and marine ecosystems for the global ocean and the European seas. CMEMS includes both satellite and in-situ high-level products prepared by Thematic Assembly Centres (TACs) and modelling and data assimilation products prepared by Monitoring and Forecasting Centres (MFCs). The Ocean Colour Thematic Assembly Centre (OCTAC) builds and operates the European ocean colour operational service within CMEMS providing global, Pan-European and regional (Arctic Ocean, Atlantic Ocean, Baltic Sea, Black Sea, and Mediterranean Sea) ocean colour (OC) products based on earth observation from OC missions (Le Traon 2015, Von Schuckman 2017). The OCTAC bridges the gap between space agencies, providing ocean colour data, and all users that need the added-value information not available from space agencies. Presently, the OCTAC relies on current and legacy OC sensors: MERIS, from ESA, SeaWiFS and MODIS from NASA, VIIRS from NOAA, and most recently on the Copernicus Sentinel 3A OLCI sensor.

Starting from the Level-2 (L2) data downloaded from space agencies, the OCTAC generates Level-3 (L3) and Level-4 (L4) products in near-real time (NRT), delayed time (DT). L3 products refer to the single snapshot, or daily combined products, mapped onto a regular grid, while L4 are products for which a temporal averaging method and/or an interpolation procedure is applied to fill in missing data values. The NRT products are operationally produced daily to provide the best estimate of

5   the ocean colour variables at the time of processing. These products are generated soon after the satellite swaths are available together with climatological ancillary data, e.g., meteorological and ozone data for atmospheric correction, and predicted attitude and ephemerides for data geolocation. In the DT processing, the updated ancillary data made available from the space agencies are used to improve the quality of the NRT data. NRT and DT data streams hence are designed to fulfil the operational oceanography specific requirements for near real time availability of high quality satellite data with a sufficiently

10   dense space and time sampling (e.g., Le Traon et al., 2015). Generally, once a year, the full data time series undergoes a reprocessing (REP) to ensure most recent findings to be consistently applied and back propagated to all data. REP products are multi-year time series produced with a consolidated and consistent input dataset and processing software configuration, resulting in a dataset suitable for long-term analyses and climate studies (Von Schuckman et al., 2017, Sathyendranath et al., 2017 and references therein).

15   Within CMEMS, following the "One Question One Answer" approach of operational satellite oceanography, observations from multiple missions are processed together to ensure homogenized and inter-calibrated datasets for all essential ocean variables. Moreover, multi-sensor products benefit of a higher coverage also providing users with less ambiguous source of information as compared with the single-sensor approach. Currently in the OCTAC, the NRT and DT multi-sensor L3 and L4 products are derived from MODIS-AQUA and NPP-VIIRS data, while REP includes observations from SeaWiFS,

20   MODIS-AQUA, MERIS and NPP-VIIRS. Global REP products derive from two datasets: the OC-CCI (Climate Change Initiative, www.esa-oceancolour-cci.org) funded by the European Space Agency and the Copernicus-GlobColour initially developed by Globcolour Project (www.globcolour.info) and then updated and produced in the framework of CMEMS. OLCI is foreseen to be included into the NRT/DT multi-sensor products in 2018 and in the REP when the quality of the data will be deemed suitable.

25   In general, DT and REP products are meant to answer different questions and to satisfy different needs such as assimilation into operational models and climate studies, respectively. As such DT need to be timely and precise while REP data are expected to be stable in time, consistent and both to be accurate. In name of the timeliness, the accuracy of the NRT-DT data is relaxed with respect to the one associated with REP time series. In this respect, one of the aims of this work is to propagate the REP configuration to the DT processing mode, allowing full compatibility between the two datasets and to extend the

30   climate-fit-research to the most recent observations.

Regional products differ from their global counterparts as they are specifically derived to accurately reflect the bio-optical characteristics of each basin (e.g., Szeto et al., 2011; Volpe et al., 2007; Pitarch et al., 2016; D'Alimonte and Zibordi, 2003). Due to peculiarities in the optical properties, the Mediterranean Sea oligotrophic waters are less blue (30 %) and greener (15 %) than the global ocean (Volpe et al., 2007), causing an overestimation of the phytoplankton chlorophyll concentration

(CHL) retrievals by standard global algorithms (e.g Bricaud et al., 2002, D'Ortenzio et al., 2002). In the last decade, more accurate regional bio-optical algorithms (e.g., MedOC4) were implemented in the single-sensor operational processing chains for the Mediterranean Sea (Santoleri et al., 2008; Volpe et al., 2012).

This work describes the main processing steps, the validation framework and results for the multi-sensor L3 product for the
5   Mediterranean Sea, operationally performed within CMEMS by the Group for Global Ocean Satellite monitoring and marine ecosystem study (GOS) in Rome, Italy. Next section (Data and Methods) describes the bio-optical dataset forming the basis for the development and validation of the regional algorithms for the Mediterranean Sea, an update of the MedOC4 parameterization, as well as the satellite data input and output of the operational processing chain. The section Results and Discussion gives an overview of the validation results obtained in the comparison between the multi-sensor satellite products
10 and the in situ data. In Conclusions section we discuss the most important achievements with relevant concluding remarks and provide future perspectives.

Data and Methods

The Mediterranean Sea in situ bio-optical dataset: MedBiOp

The development of geophysical products that best reproduce the Mediterranean biogeochemical conditions relies on the in
15 situ bio-optical dataset collected across the basin over twenty years (Figure 1). Several parameters are routinely measured both for general oceanographic purposes (e.g., water temperature, salinity, Oxygen content, fluorescence and light attenuation) and for the calibration and validation of remote sensing data, which include phytoplankton pigment concentration via HPLC (High Performance Liquid Chromatography), light absorption due to coloured dissolved organic matter (CDOM), to algal and non algal particles as well as to total suspended matter (TSM), and both inherent and apparent
20 optical properties.

In the OC processing chain the primary parameters used to derive the geophysical products is the spectral Remote Sensing Reflectance (Rrs). Here, the most important objective of using the radiometric measurements is to derive surface, above-water remote sensing Reflectance (Rrs) spectra from in-water profiles.

The multispectral Satlantic profiling system (OCR-507) is made for measuring the upwelling radiance, $Lu(z,\lambda)$, the
25 downward and the upward irradiance, $Ed(z,\lambda)$ and $Eu(z,\lambda)$, and includes a reference sensor for the downward irradiance, $Es(0,\lambda)$, mounted on the uppermost deck of the ship. A Sea-bird CTD and a tilt sensor are also part of the system. The radiometric measurements are acquired and processed following the method described in Zibordi et al. (2011). In order to increase the number of samples per unit depth, data are acquired using the multicast technique (D'Alimonte et al., 2010; Zibordi et al., 2004). Data processing is achieved using the Multi-level Elaboration software for Radiometers Data
30 Acquisitions (MERDA), developed at GOS.

The processing steps follow the consolidated protocols for data reduction of in water radiometry (Mueller and Austin, 1995; Zibordi et al., 2011). First, data are converted from digital counts into their physical units. A filter is applied to remove data

with profiler tilt angle larger than 5°. In order to reduce the influence of the light variability during the measurements, data from each sensor are normalised with the above-water downwelling irradiance. A least-square linear regression is performed on the log-transformed normalised data, whose slope determines the diffuse attenuation coefficients (Kl(λ), Ku(λ) and Kd (λ)) and the exponents of the intercept are the sub-surface quantities (Lu(0−, λ), Eu(0−, λ) and Ed(0−, λ)). Outliers due to wave

5 perturbations are removed and identified in those points differing, by default, more than two standard deviations from the regression line. The depth layer normally considered as relevant for the extrapolation is 0.3-3m, but can be changed on the basis of the characteristics of each profile. The upwelling sub-surface quantities (i.e. Lu(0−, λ), Eu(0−, λ)) are also corrected for the self-shading effect following Zibordi and Ferrari (1995) and Mueller and Austin (1995) using the ratio between diffuse and direct atmospheric irradiance, and the sea-water absorption. Using the primary sub-surface quantities is then

10 possible to derive additional products as the Q-factor at nadir (Qn(0⁻,λ)=Eu(0⁻,λ)/Lu(0⁻,λ)), the remote sensing reflectance (Rrs(λ)=0.543·Lu(0−,λ)/Es(0,λ)) or the normalized water-leaving radiance (Lwn(λ)=Rrs(λ)·E0(λ) with E0(λ) being the extra-atmospheric solar irradiance; Thuillier et al., 2003).

Fluorimetric measurements associated with CTD casts are used to increase the depth resolution of the HPLC-derived chlorophyll. These calibrated fluorimetric casts are then used to compute the optically weighted pigment concentration

15 (OWP) as already reported in Volpe et al. (2007). In addition to the MedBiOp dataset collected by GOS over the Mediterranean Sea, two fully independent datasets, collected at fixed location, are included for the validation: Rrs data estimated from above-water measurements at the Aqua Alta Oceanographic Tower (AAOT) as part of the AERONET-OC network in the northern Adriatic Sea (Zibordi et al., 2009), as well as Rrs and Chl data from the BOUSSOLE buoy located in the Ligurian Sea (Antoine et al., 2008; Valente et al., 2016).

20 **Satellite Data Processing Chain**

As mentioned, GOS operates two different processing chains (Figure 2), for the near-real time and for the reprocessed data production, respectively. The input of both processing chains is the spectral Rrs downloaded from upstream data providers, e.g., the space agencies. Hence, in both cases, the atmospheric correction is not part of these processing chains.

As schematically shown in Figure 2, the NRT/DT chain consists of four parts aimed at populating a two-year rolling archive

25 with multi-sensor Level-3 data at daily temporal resolution. These data are homogeneous in terms of format and processing software, meaning that if, for any reason, a change is made on the processing chain, the entire rolling archive is processed back for consistency. This chain involves the pre-processing of different sensors with different wavelengths (as detailed in Single sensor pre-processing section) that are then merged together over a common set of wavelengths (Table 1, section Multi sensor processing: Rrs spectra). The Level-3 geophysical products section provides a description of the algorithms for

30 the derivation of Chlorophyll Concentration (Chl, in units of mg m^{-3}) and of the attenuation coefficient of light at 490 nm (Kd490, in units of m^{-1}). As it will be detailed later, the inherent optical properties (IOPs: the absorption due to phytoplankton, a_{ph}, and to detrital and dissolved matter, a_{dg}, and the backscattering due to particles, b_{bp}, all at 443 nm) are

used to align the different sensors over the common set of wavelengths. For this reason, the IOPs are an active part of the processing and are also made available to users as output of the chain.

For the REP processing, Rrs spectra are already available at those wavebands, as the entire data time series is processed with a consistent configuration, providing users with the longest and most consistent available data time series, spanning over

5 twenty years (1997 to 2017), for the Mediterranean Sea. Within CMEMS, the spectral Rrs is produced by the Plymouth Marine Laboratory (PML), which uses the OC-CCI processor version 3 (www.esa-oceancolour-cci.org) to merge at 1km resolution (rather than at 4km as for OC-CCI) MERIS, MODIS-AQUA, SeaWiFS and VIIRS data; this dataset is hereafter referred to as CCIv3. At the moment of writing, the CCIv3 is based on the NASA reprocessing 2014.0. These data are updated on a yearly basis and are available to users on the CMEMS web portal (marine.copernicus.eu). The outputs of the

10 REP chain are the Chl and Kd490, consistently retrieved with the same algorithms as in the NRT/DT chain.

For consistency, the wavelengths at which the Rrs spectra are provided to users are the same for both processing chains (REP and NRT/DT). Similarly, for compatibility, the same Chl and Kd490 algorithms are used in both processing chains (section Level-3 geophysical products).

Single sensor pre-processing

15 Once downloaded and quality checked, single-sensor L2 data (R2018.0 for SeaWiFS, MODIS-AQUA and VIIRS; third reprocessing for MERIS) are fed into the pre-processing chain to harmonize data from different sensors in terms of format, projection, and most of all in terms of a common set of wavelength bands. Moreover, the pre-processing also takes care of sorting out issues that may affect one sensor only.

Destriping

20 An important task, operationally performed over both MODIS-AQUA and NPP-VIIRS images is the application of a destriping procedure over L2 products to remove the instrument-induced stripes. These two sensors scan the Earth surface via a rotating mirror system which reflect the surface radiance to band detectors. Stripes derive from two hardware problems: i) the two sides of the mirror are not exactly identical, and ii) the band detector degradation is not homogeneous. Destriping correction is performed by applying the method developed by Bouali and Ignatov (2014) and adapted to ocean colour

25 products by Mikelsons et al. (2014). The procedure splits the image into a striped component and a stripe-free component. The striped component is then passed through a filter to eliminate the stripes, and then is added back to the stripe-free component to produce the final destriped image. The definition of striped and de-striped domains is achieved by measuring the gradients (both along and across the scan) and by selecting as "stripped" the ones below the pre-determined threshold values.

30 *Removal of the bowtie effect*

VIIRS data suffer of the bowtie effect. Sensor detectors have constant angular resolution so that the sampled Earth area, i.e. the dimension of the pixel at ground, increases with the scan angle. This results in consecutive scans to overlap away from nadir, in turn giving the entire scan the shape of a bowtie. The processing performed by space agencies generally removes

this effect in each VIIRS granule through a combination of aggregation and deletion of overlapping pixels, resulting in a series of rows of missing values at the edge of each L2 granule. In this production chain, these missing values are filled in by linear interpolation.

Flagging & Mosaicking

5   Each L2 granule is quality checked via the application of the L2 flags provided by Space Agencies. The flags applied to both MODIS and VIIRS are those of the standard processing from space agencies (https://oceancolor.gsfc.nasa.gov/atbd/ocl2flags/), except for the atmospheric correction failure flag that is not applied to VIIRS for avoiding too many false positive pixels to be rejected. Moreover, to remove the "salt and pepper" effect, each granule undergoes a further quality check by removing all isolated pixels and by filling in all isolated missing pixels using

10   the near-neighbourhood approach. All Rrs spectra are further checked for the presence of negative values, which may occur in the blue part of the spectrum due to the failure of the atmospheric correction; one negative value within the spectrum (excluding the NIR bands) is enough for the entire spectrum to be rejected. All available granules for each day are remapped on the Equirectangular grid covering the Mediterranean Sea. All re-gridded granules from the same sensor and from the same day are mosaicked together into a single file containing the Remote Sensing Reflectance at nominal sensors'

15   wavelengths.

Band-shifting

At the scale of the pixel, the goal is to merge single-sensor Rrs spectra into a single spectrum. The idea is that from the Rrs spectrum one can easily derive, directly or indirectly, all the geophysical parameters of interest not only for the ocean colour community, but also for the wider biogeochemical scientific community. One of the problems of the multi-sensor merging is

20   the different set of bands of the various ocean colour sensors that have to be merged. Some bands are coincident (443 nm), others may differ of a few nanometres (486 and 488 or 410 and 412 nm) while others can be significantly different (e.g., the green bands of MODIS-Aqua, SeaWiFS and OLCI, which are 547nm, 555nm and 560 nm respectively, Table 1). A technique to collapse the various spectra on a pre-defined set of bands is thus essential for the multi-sensor merging; to this aim the band shifting method described by Melin and Sclep (2015) was implemented here with the application of the Quasi

25   Analytical Algorithm (QAA, Lee et al., 2002) in forward and backward modes. In general, Rrs is related to the absorption and scattering properties of the medium, which in turn are given by the additional contributions of all the medium components (seawater, particulate and dissolved matters). Starting from the Rrs at the sensor native wavelengths and from the characteristic spectral shapes of the IOPs, the QAA allows the estimation of the IOPs at target wavelengths. The QAA is then applied in forward mode to estimate the Rrs at these bands. This approach produces a set of common bands (grey-

30   shaded in Table 1) for all sensors and allows, in theory, the daily merging of the Rrs from which it is then possible to apply the algorithms to derive the geophysical products. The uncertainty induced by band shifting is estimated in most cases at well below 5% of the reflectance value (with averages of typically 1–2%), especially for open ocean regions (Mélin and Sclep, 2015).

Multi sensor processing: Rrs spectra

Once single sensor spectra are homogeneous in terms of wavebands it is possible for the Rrs from the available sensors to be merged together into single images. The output is a set of six Rrs images, each of which is treated as an individual image independently from the other Rrs bands of the spectrum. In other words, we move from the wavelength domain in which each pixel is associated with a common set of Rrs bands (a spectrum), to the spatial domain in which the aim is to assign a value to all pixels that were validly sampled, independently from the sensor that actually acquired the observation.

Differences between MODIS and VIIRS

At pixel scale, several reasons can be at the base of the differences between two observations. The geometry of the observations constitutes an issue that is under the control of the atmospheric correction scheme. Since this part of the processing is performed by space agencies, this issue is rarely accounted for in the context of L3 multi-sensor merging, which instead only considers the radiometric quantities as fully normalized (Maritorena and Siegel, 2005). The order of magnitude difference between Rrs retrieved by MODIS and VIIRS is approximately 10%, although not uniformly distributed through the entire visible spectrum, and with MODIS being in general above VIIRS. Rrs at 490 nm displays the narrowest spread around the line of best agreement and lower than 10%, whereas other bands show wider distribution reaching values of about 15% difference (data not shown). Moreover, a pixel is sampled with different geometry (scattering angle) and not exactly at the same time by the two sensors; in the Mediterranean Sea, the differences between the two sensor time overpasses do not exceed one hour. Here, we tested that approximately 10% difference between the two Rrs spectra cannot be ascribed to differences in the overpass times and/or to the geometry of the observation, and that it must be due to inter-calibration issues, which must be addressed before any sensor merging can effectively be performed (Sathyendranath et al., 2017).

Inter-Sensor Bias Correction

Here, we extend the method developed by Melin et al. (2017) within OC-CCI for reducing the inter-sensor bias, as this is a propedeutical step to the proper merging of data collected from different sensors. In practice, when two or more sensors are available for the same period, one sensor is taken as reference and the others are bias-corrected to the reference. For the inter-sensor bias to be corrected, daily climatological bias maps are computed at the same spatial resolution of the source data (e.g., 1 km). During the SeaWiFS era, the method is applied to SeaWiFS-MODIS-MERIS sensors having SeaWiFS as reference. From 2010 onward, the method is applied to the couple MODIS-VIIRS using MODIS as reference, after its bias with SeaWiFS is corrected. The way the bias is here computed differs from the OC-CCI technique in two steps: i) the first temporary seven-day average (from three days prior to three days after the day of interest), ii) the averaging method for estimating the climatology maps and iii) this method was not applied to the 670 nm band. The seven-day average is computed to enhance data coverage and, rather than a simple average, here it is derived using a weighted-averaging function that gives more importance to the data day with respect to those that are away from it. The equation for computing the daily climatology over the 2N+1 days (with N=3) is:

$$\delta(d,x,y) = \frac{\sum_{i=-N}^{N} w_i \delta_i(d+i,x,y)\theta_i}{\sum_{i=-N}^{N} w_i \theta_i},$$ (1)

with

$$w_i = \frac{N+1-|i|}{N+1},$$ (2)

where $\delta(d,x,y)$ is the daily climatology, and $\theta_i = 1$ if δ_i is associated with a valid value, zero otherwise. The value of the

5 weight decreases from 1, for the same day of the climatology, to 0.75 (N/N+1) for the days before and after, to 0.25 (1/N+1) for the first and last days of the ±3-day window.

As for the averaging method for computing the climatology map, we applied a weighting-function not only in the time dimension but in both space and time, contemporaneously. As for the OC-CCI, the time window is set to 60 days. The spatial kernel of the 3x3 box centred to the pixel is defined as:

0.25	0.50	0.25
0.50	1.00	0.50
0.25	0.50	0.25

10 The cumulative effect of these two weighting functions is given by their cross product.

The method was not applied to the 670 nm band because the quality of the SeaWiFS retrievals in this part of the spectrum was deemed insufficient. First, the number of matchups between SeaWiFS and all the available in situ data (MedBiOp, BOUSSOLE and AAOT) at 670 nm is ~40% of those in the blue-green spectral region (data not shown). Furthermore, as better detailed later, the percent difference between SeaWiFS and in situ observations (at 670 nm) is one or two orders of

15 magnitude larger than the blue-green counterparts in both oligo- and meso-trophic conditions (MedBiOp, BOUSSOLE).

Before merging all the available sensors together at any given time, their Rrs spectra are individually bias-corrected with respect to their references, as detailed above with the exception of the 670 nm band for which a simple average is applied.

Sensor-Merging

When merging data from two or more sensors, three possible conditions can occur: i) the pixel is observed from more than

20 one sensor, ii) the pixel is observed from one sensor only, iii) the pixel is in no clear sky condition or masked out because of any of the operational L2 flags, from all sensors. In the latter case the pixel is assigned the missing value. In the former two conditions the method is not straightforward because it strongly depends on the ability to reduce the inter-sensor bias to zero. When the pixel is sampled by one sensor only, but the surrounding pixels by more than one or by the other sensors, there is an increasing probability of introducing artefacts or spatial gradients, which in reality do not exist and are only given by the

25 merging procedure. To prevent the occurrence of such horizontal discontinuities, here we apply the smoothing procedure based on the use of the climatology field described in Volpe et al. (2018). First, the field from each sensor (Figure 3a-b) is filled with the same relevant daily climatology (Figure 3e, see below for more details), as shown in Figure 3c-d. This enables the average of these two (or more) fields to be easily computed. All the non-observed pixels are then set to the missing value (Figure 3f). This is the procedure operationally and currently applied to data acquired by MODIS-AQUA and VIIRS to

produce the multi-sensor Rrs product. It is important to note that features, which are only present in the climatology, but not in the daily single-sensor images, are also absent in the merged product. In the example of Figure 3, features of such a kind can be clearly identified in correspondence of the Strait of Bonifacio, in the Tyrrhenian Sea, which extends towards the west coast of Italy only in the climatology but in none of the other fields (MODIS-AQUA or VIIRS). Another example is given

5   by the tongue of Modified Atlantic Water (Manzella et al., 1990) that penetrates the southern sector of the Sicily Channel towards the Libyan coasts, which is present in AQUA, VIIRS, and in the merged image, but not in the climatology. Similarly, the Rhone River plume, visible in the climatology, is absent from both single-sensor images and from the merged multi-sensor product.

After all bands are merged, single pixel Rrs spectra are available (Figure 4) for the geophysical products to be computed.

10   Within this step, a mask is computed for keeping track of the single sensor inputs to the multi-sensor product and added to the NetCDF files (Figure 4b and Figure 4d). The examples show two cases of blue and greener waters along the Spanish coast and in the northern Adriatic Sea, respectively. In both cases, the bias correction demonstrates to improve the satellite Rrs estimate being closer to the in situ measurements, at all bands.

Climatology

15   As mentioned the climatology provides a spatial support to the sensor merging. The climatology field is obtained from the thirteen years of SeaWiFS data using the MedOC4 regional algorithm for CHL (Volpe et al., 2007). This daily field has the same spatial resolution (nominally 1 km at nadir) and projection (cylindrical) as the operational field. These climatology maps were created using the data falling into a moving temporal window of ± 5 days. Five days are deemed to be a good compromise between the need of filling the spatial domain and the de-correlation time scale of the OC data in the

20   Mediterranean Sea; this has been estimated as being 3 days on average (the day at which the autocorrelation value halves). One of the main purposes of a climatology field is to serve as reference, and as such it is expected to be as reliable as possible, thus avoiding biases caused by single incorrect pixel values. To overcome these possible biases, a filtering procedure is applied to the entire SeaWiFS time series, by removing all isolated pixels and by filling in all isolated missing pixels using the near-neighbourhood approach. The resulting daily climatology time series includes the pixel-scale standard

25   deviation, the average, the median, the modal, the minimum, and the maximum values.

Level-3 geophysical products

The first output of the processing chain is the Rrs spectrum derived from the method described above, and that constitutes the input to all algorithms used to derive the various geophysical products. As shown in Figure 2, from this point on, the NRT and the REP chains collapse as they both use the same algorithms for computing Chl, Kd and the IOPs. Next sections

30   explain how the various algorithms are derived and applied to Rrs data for their operational application.

Chlorophyll a concentration

There are two main categories of Chl algorithms, empirical and semi-analytical. Despite the latters became mature enough to be often compared to the performances of the empirical algorithms, these still remain more robust and are generally preferred

in the operational context (e.g., NASA processing). Recently, in the context of what are the best characteristics that data must have to be used in climate studies, Sathyendranath et al. (2017) pointed out that, despite theoretical algorithms (semi-analytical) are preferred to empirical ones (they rely on past observations, which are not necessarily the best approximation for future observations, as shown in Dierssen, 2010), they still lack the robustness, which is typical of the OC4-family of

5   algorithms (OReilly et al., 2000 among others).

Operational services such as CMEMS aim at providing data for a wide range of applications from the assimilation of open ocean observations into biogeochemical models (Teruzzi et al., 2014) to coastal monitoring programs (such as the Marine Strategy Framework Directive, e.g. Colella et al., 2016). Unfortunately, there is not yet a unique Chl algorithm able to perform with the same accuracy across water types. Since the offshore extension of the coastal waters may vary and be of

10   several kilometres (pixels), depending on the sea and whether conditions (e.g., coastal filaments may extend several tens of kilometres in the open ocean), the adoption of static masks for the application of different algorithms would result in errors associated with the sharp fronts. One way to overcome this issue is to merge two Chl products into a single field, after the exact identification of the two realms (Mélin et al., 2011; Volpe et al 2012; Moore et al., 2014). At pixel scale, Rrs spectra are translated into Chl twice: assuming the entire satellite scene to belong to Case I and to Case II waters, each with its own

15   algorithm. Then, to identify the pixels belonging to Case I and Case II conditions, the identification of the two water types relies on the in situ reference Rrs spectra as fully described in D'Alimonte et al. (2003). For the computation of these two average spectra two distinct datasets were used; for Case I and Case II waters the MedOC4 (Volpe et al., 2007) and CoASTS (Berthon et al., 2002, Zibordi et al., 2002) datasets are used, respectively. This approach is one step towards the need of the scientific community of dealing with products performing equally well in both water types, or at least to know where the

20   first ends and the second starts (Sathyendranath, 2011, OC-CCI user consultation). To address also the latter point evidenced by the user survey, a water type mask resulting from the Case I-Case II merging step is conveniently stored into the NetCDF files and made available to users. Thus two different algorithms are used to derive Chl in the two optical domains: the ADOC4 algorithm (D'Alimonte and Zibordi, 2003) is used for the Case II domain, while algorithm for Case I constitutes the matter of the next paragraph.

25   *Mediterranean Sea – MedOC4 – Case I*

The algorithm used to retrieve Chl in the Case I waters of the Mediterranean Sea is an updated version of the MedOC4, a regionally parameterized Maximum Band Ratio (Volpe et al., 2007). Figure 5a shows both the regional and the global algorithm (OC4v6, https://oceancolor.gsfc.nasa.gov/atbd/chlor_a/) functional forms superimposed to the in situ observations collected in the Mediterranean Sea. The Mediterranean Sea tends to be "greener" than the Pacific and Atlantic oceans for any

30   CHL values due to higher CDOM concentrations (Volpe et al., 2007 and references therein). Considering that the empirical algorithms are the expression of the in situ data from which they are derived, this figure provides a means for understanding the need to regionalize the algorithms to avoid the significant Chl overestimation that would be obtained with the global algorithm, as already fully documented in Volpe et al. (2007, and references therein).

An important point that has to be borne in mind is that the colour of the ocean, in terms of maximum band ratio, explains 74% of the entire phytoplankton variability, as expressed by the chlorophyll concentration. This points to the importance (more than 20%) of the second order variability of the ocean colour signal (Brown *et al.*, 2008) that should be accounted for by future versions of the operational algorithms, in line with the recent recommendation about the use of ocean colour data

5 for climate studies (Sathyendranath et al., 2017).

Diffuse Attenuation Coefficient - Kd490

The algorithm used to compute the diffuse attenuation coefficient of light at 490 nm is a fourth power polynomial expression of the Rrs ratio (R=Rrs490/Rrs555) as already done at global scale (https://oceancolor.gsfc.nasa.gov/atbd/kd_490/). A subset of the in situ bio-optical dataset used for Chl is used to compute the algorithm for the retrieval of Kd490. Figure 5b shows

10 both the regional and the global algorithm functional forms superimposed to the in situ observations collected in the Mediterranean Sea. All the available Kd490 observations from the CNR in situ dataset were used for the development of the algorithm so that we are unable of performing an independent validation.

Validation framework

The validation of the satellite products was carried out by pairwise comparison with the in situ observations: Chl, apparent

15 (Kd490 and Rrs) and Inherent Optical Properties (absorption and backscattering coefficients). For determining co-location between in situ and satellite data records all measurements acquired in the same day were used, as L3 data used in this study does not preserve the time information. It should be noted that, as only day-light in situ measurements were used, the Bailey and Werdell (2006) narrow time window for determining coincidence (i.e. no more than ± 3 h) is met in most instances. Then, similarly to Zibordi et al. (2012), the median values is extracted from a 3 by 3 box centred on the in situ measurement

20 coordinates, only if at least 5 pixels have valid values and the coefficient of variation is smaller than 20%.

The uncertainty associated with the in situ data is due to several factors, e.g., the sea conditions, the operator ability which in turn can introduce several contamination factors; hence, here we consider satellite and in situ observations to be both affected by uncertainties (Loew et al., 2017). Thus, for the matchup analysis, a type-2 regression (also called orthogonal regression) is implemented here (Laws and Archie, 1981). The statistical parameters for the assessment of satellite versus in

25 situ data are listed in Table 2. For log-normally distributed variables (such as Chl) both datasets are log-transformed prior to computing the metrics. A good match between the two observations is achieved when S is close to one and I is close to zero. The RMSD is the average distance of a data point from the fitted line, measured perpendicular to the regression line. RMSD and bias have the same units as the data from which they are derived.

Results and Discussion

30 This section provides the validation analysis for the operational NRT retrievals of Rrs and Chl with the multi-sensor merged approach (Multi). The NRT products (Multi) are available in the CMEMS catalogue as a rolling archive spanning two years,

prior which REP products are available instead. Since most of the in situ data used for the validation analyses were collected earlier than 2016 (two years ago, at the time of writing), we used the NRT production chain to process the entire satellite data archive. As reference we also included validation of the OC-CCI-based REP products.

Temporal trend

5   In this context and with the general aim of identifying any temporal dependence of the computed statistics, the analysis was made comparing the satellite products with space-time collocated in situ measurements for each campaign separately and for the whole dataset. No significant temporal behaviour emerged from the analysis (results not shown), highlighting that both in situ and satellite data are homogeneous in time and well calibrated. Similar results were recently yielded at global scale by Sathyendranath et al. (2017).

10   *Matchup – Rrs single-sensors, multi-sensor*

Figure 6 shows the relative difference between satellite and the MedBiOp Rrs spectra. Satellite Rrs at all available bands for each sensor are compared with the same in situ Rrs bands (Table 1). There is a common spectral behaviour between satellite and in situ observations, with the Rrs in the blue bands (443 and 490 nm) performing better than those at 412 nm or those in the green region (510 and 555 nm). Apart from the 670 nm band (56%), SeaWiFS performs generally better than the other

15   sensors, thus supporting the choice of being selected as reference sensor for the blue-green spectral range. All other satellite data never exceed 15% difference when compared with in situ observations at basin scale. A noticeable feature presented in Figure 6 is the wide variability of the computed statistics (given by the standard deviation bars) highlighting that the satellite data presented here do not significantly differ from the in situ observations. Table 3 shows the full statistics for the Multi Rrs product.

20   One of the main reasons for merging data from different sensors is to enhance the domain coverage by reducing the influence of both the cloud coverage and generally flagged or masked pixels as well as the out-of-satellite-swath areas; in all cases the use of a multi-sensor approach increases the probability of valid clear sky observations. Figure 7 shows the time series of the percent basin coverage for three single sensors (MODIS-AQUA, VIIRS and SeaWiFS) and of the multi-sensor product. The number of clear sky pixels of the multi-sensor is on average larger than that of each single sensors by as much

25   as 20%, with minimum impact during winter and maximum at summertime. The difference between periods of maxima and minima somehow reflects the cloud cover influence over the multi-sensor product, with the winter-time being characterized by both cloud-cover and out-of-satellite-swath, while the summer periods being mostly affected by out-of-satellite-swath masked areas.

Results in Figure 6 are representative of the performances of the various satellite observations (both single- and multi-

30   sensors) against the in situ measurements that were widely collected over the basin in the past twenty years, the MedBiOp dataset. Similarly, Figure 8 shows the comparison of the two multi-sensors time series (Multi and CCIv3) against three in situ datasets: the basin scale dataset (MedBiOp) and two fixed location datasets, one of which coastal (AAOT). In general, one could expect the mismatch between satellite and in situ observations to be larger at the extreme bands of the spectrum: 412 nm and 670 nm. In the first case, because of the spectral distance from the NIR bands used for the atmospheric

correction, and in the second because of the generally very low Rrs values that pose a challenge for both in situ and satellite determination of the Rrs at this band. The difference between satellite and in situ Rrs observations at these extreme bands is of the same order of magnitude as the blue-green part of the spectrum when observed in open ocean (MedBiOp and BOUSSOLE), while it appears significant in the coastal domain (AAOT). The use of the NASA reprocessing (R2018.0) in

5   the Multi but not in the CCIv3 (R2014) is the likely cause for the different performances in the blue region. In the NIR region, the spread of results between different satellite data among the three in situ reference observations is largest. One reason can be given by the large difference in the number of used matchups (Table 4). Overall, despite their absolute differences the two multi-sensor satellite products show a similar level of accuracy which suggest the use of the Multi also for the REP products. This would provide the two benefits of reducing the number of upstream data provider and of giving

10   the NRT and REP products full compatibility.

Matchup – Chl

Figure 9 shows the matchups for the L3 Chl product for both processing modes, REP (derived from the CCIv3 Rrs) and NRT (derived from the multi-sensor merged described in this study). Both products are regularly distributed around the line of best agreement for the entire Chl range, although for in situ values larger than 0.3 mg m^{-3} there is a noticeable dispersion

15   increase. Table 5 shows the statistics of the four datasets plotted in Figure 9. To asses the uncertainties of the Multi Chl currently distributed on the CMEMS portal, the analysis was performed on the period in which VIIRS and MODIS co-exist, i.e. November 2011 onwards. There is a significant difference between the biases computed when the most recent observations are used (REP$_{AV}$ and Multi$_{AV}$) and over the entire time series, likely due to the number of matchups (44 vs 708) and range of Chl values (~0.04-2 vs ~0.007-9) associated with the bio-optical and trophic regimes (Figure 1).

Conclusions

This work presented the latest achievements in the operational processing chain for ocean colour data stream for the Mediterranean Sea in the context of the European Copernicus Marine Environment Monitoring Service. The development of the multi-sensor merged product builds on the previous version of this chain, which was focused on parallel processing of

25   single sensors (SeaWiFS, MODIS and MERIS, Volpe et al., 2012). Three main steps were implemented: band-shifting, inter-sensor bias correction, and the sensor merging. The band-shifting is implemented exactly as in Melin and Sclep (2015), while the implementation of the inter-sensor bias correction differs from the OC-CCI technique (Melin et al., 2017) in the temporal and spatial aggregation scales. The sensor-merging shown in this work is based on the use of the climatology as input to the smoothing procedure as described in Volpe et al. (2018). The output of this processing chain is the Rrs spectrum

30   that constitutes the input to all algorithms used to derive the various geophysical products. The Rrs computed with the multi-sensor merged approach shows good agreement when compared with in situ observations of the basin-scale MedBiOp dataset as well as the two fixed location AAOT and BOUSSOLE time series. Moreover, this work presents an updated

version of the empirical algorithms for Chl and Kd retrievals for the Mediterranean Sea based on the extended MedBiOp dataset. The comparison with the in situ observations yields good results when applied to both the Rrs derived from the CCIv3 processor and those derived from the multi-sensor merged processing shown here. This suggests the opportunity to use the proposed multi-sensor processing chain in the REP context as well.

5 **Acknowledgement**

References

Antoine, D., Guevel, P., Desté, J.-F., Bécu, G., Louis, F., Scott, A., and Bardey, P., 2008. The "BOUSSOLE" Buoy – A New Transparent- to-Swell Taut Mooring Dedicated to Marine Optics: Design, Tests, and Performance at Sea. J. Atmos. Oceanic Technol., 25, 968–989.

10 Bailey, S.W., Werdell, P.J., 2006. A multi-sensor approach for the on-orbit validation of ocean color satellite data products. Remote Sens Environ., 102, 12–23.

Berthon, J. F., G. Zibordi, Doyle, J.P., Grossi, S., van der Linde, D. Targa, C., 2002. Coastal Atmosphere and Sea Time Series (CoASTS), Part 2: Data Analysis. NASA Technical Memorandum. 2002-206892 Vol. 20. S. B. Hooker and E. R. Firestone. Greenbelt, Maryland, NASA Goddard Space Flight Center: 25.

15 Bouali, M., and Ignatov, F., 2014. Adaptive Reduction of Striping for Improved Sea Surface Temperature Imagery from Suomi National Polar-Orbiting Partnership (S-NPP) Visible Infrared Imaging Radiometer Suite (VIIRS), J. Atmos. Oceanic Technol., 31, 150-163.

Bricaud, A., Bosc, E., & Antoine, D., 2002. Algal biomass and sea surface temperature in the Mediterranean Basin - Intercomparison of data from various satellite sensors, and implications for primary production estimates. Remote Sensing of 20 Environment, 81(2–3), 163–178.

Brown, A.C., Huot, Y., Werdell, P.J., Gentili, B., Claustre, H., 2008. The origin and global distribution of second order variability in satellite ocean color and its potential applications to algorithm development. Remote Sensing of Environment, 112, 4186–4203.

Colella, S., Falcini, F., Rinaldi, E., Sammartino, M., Santoleri, R., 2016. Mediterranean Ocean Colour Chlorophyll Trends. 25 PLoS ONE 11(6): e0155756. https://doi.org/10.1371/journal.pone.0155756.

D'Alimonte, D. and Zibordi, G., 2003. Phytoplankton Determination in an Optically Complex Coastal Region Using a Multilayer Perceptron Neural Network, IEEE Geosci. Remote S., 41, 2861–2868.

D'Alimonte, D., Mélin, F., Zibordi, G., Berthon, J.-F., 2003. Use of the novelty detection technique to identify the range of applicability of the empirical ocean color algorithms. IEEE Trans. Geosci. Remote Sens., 41, 2833-2843.

30 D'Alimonte, D., Zibordi, G., Kajiyama, T., Cunha, J.C., 2010. Monte Carlo code for high spatial resolution ocean color simulations, Applied Optics 49, 4936-4950.

Dierssen, H., 2010. Perspectives on empirical approaches for ocean color remote sensing of chlorophyll in a changing climate. Proc. Natl. Acad. Sci. 107, 17073–17078.

D'Ortenzio, F., Marullo, S., Ragni, M., D'Alcalà, M. R., & Santoleri, R., 2002. Validation of empirical SeaWiFS algorithms for chlorophyll-a retrieval in the Mediterranean Sea: A case study for oligotrophic seas. Remote Sensing of Environment, 82(1), 79–94. https://doi.org/10.1016/S0034-4257(02)00026-3.

Laws, E. A., Archie, J. W., 1981. Appropriate use of regression analysis in marine biology. Marine Biology, 65(1), 13-16.

Lee, Z.P., Carder, K.L., Arnone, B.A., 2002. Deriving inherent optical properties from water color: A multi-band quasi-analytical algorithm for optically deep waters, Applied Optics, 41, 5755-5772.

Le Traon, P-Y., Antoine, D., Bentamy, A., Bonekamp, H., Breivik, L.A., Chapron, B., Corlett, G., Dibarboure, G., DiGiacomo, P., Donlon, C., Faugère, Y., Font, J., Girard-Ardhuin ,F., Gohin, F., Johannessen, J.A., Kamachi, M., Lagerloef, G., Lambin, J., Larnicol ,G., Le Borgne, P., Leuliette, E., Lindstrom, E., Martin, M.J., Maturi, E., Miller, L., Mingsen, L., Morrow, R., Reul, N., Rio, M-H., Roquet, H., Santoleri, R., Wilkin, J., 2015. Use of satellite observations for operational oceanography: recent achievements and future prospects. Journal of Operational Oceanography, 8 (sup1), s12-s27.

Loew, A., Bell, W., Brocca, L., Bulgin, C. E., Burdanowitz, J., Calbet, X., Verhoelst, T., 2017. Validation practices for satellite-based Earth observation data across communities. Reviews of Geophysics, 55(3), 779–817. http://doi.org/10.1002/2017RG000562

Manzella, G. M. R., Hopkins, T. S., Minnett, P. J., & Nacini, E., 1990. Atlantic water in the Strait of Sicily. Journal of Geophysical Research, 95(C2), 1569–1575.

Maritorena, S., Siegel, D. A., 2005. Consistent merging of satellite ocean color data sets using a bio-optical model. Remote Sensing of Environment, 94, 429–440.

Mélin, F, and Sclep, G., 2015. Band shifting for ocean color multi-spectral reflectance data. Opt. Exp., 23, 2262-2279. DOI:10.1364/OE.23.002262.

Mélin, F., Vantrepotte, V., Chuprin, A., Grant, M., Jackson, T., & Sathyendranath, S., 2017. Assessing the fitness-for-purpose of satellite multi-mission ocean color climate data records: A protocol applied to OC-CCI chlorophyll-a data. Remote Sensing of Environment, 203, 139–151. http://doi.org/10.1016/j.rse.2017.03.039

Mélin, F., Vantrepotte, V., Clerici, M., D'Alimonte, D., Zibordi, G., Berthon, J. F., Canuti, E., 2011. Multi-sensor satellite time series of optical properties and chlorophyll-a concentration in the Adriatic Sea. Progress in Oceanography, 91(3), 229–244. http://doi.org/10.1016/j.pocean.2010.12.001

Mikelsons, K., Wang, M., Jiang, L., Bouali, M., 2014. Destriping algorithm for improved satellite-derived ocean color product imagery, Opt. Express 22, 28058-28070.

Moore, T. S., Dowell, M. D., Bradt, S., Ruiz Verdu, A., 2014. An optical water type framework for selecting and blending retrievals from bio-optical algorithms in lakes and coastal waters. Remote Sensing of Environment, 143, 97–111. http://doi.org/10.1016/j.rse.2013.11.021.

Mueller, J. L., and Austin, R. W., 1995. Ocean Optics Protocols for SeaWiFS Validation, Revision 1, S.B. Hooker, E.R. Firestone, and J.G. Acker Ed., NASA Technical Memorandum 104566, Vol. 25, SeaWiFS Technical Report Series

O'Reilly, J. E., Maritorena, S., Siegel, D., O'Brien, M. C., Toole, D., Mitchell, B. G., Culver, M., 2000. Ocean color chlorophyll a algorithms for SeaWiFS, OC2, and OC4: version 4. In S. B. Hooker & E. R. Firestone (Eds.), SeaWiFS

5 Postlaunch Technical Report Series, vol.11. SeaWiFS postlaunch calibration and validation analyses: part 3 (pp. 9–23). Greenbelt, MD: NASA Goddard Space Flight Center.

Pitarch, J., Volpe, G., Colella, S., Krasemann, H., and Santoleri, R., 2016. Remote sensing of chlorophyll in the Baltic Sea at basin scale from 1997 to 2012 using merged multi-sensor data, Ocean Sci., 12, 379-389, https://doi.org/10.5194/os-12-379-2016.

10 Santoleri, R., Volpe, G., Marullo, S., Buongiorno Nardelli, B., 2008. Open Waters Optical Remote Sensing of the Mediterranean Sea, in: Remote Sensing of the European Seas, edited by: Barale, V. and Gade, M., Springer, 103–116.

Sathyendranath, S., Brewin, R.J.W., Frédéric Mélin, T. J., Platt, T., 2017. Ocean-colour products for climate-change studies: What are their ideal characteristics?, Remote Sensing of Environment, http://dx.doi.org/10.1016/j.rse.2017.04.017

Szeto, M., Werdell, P. J., Moore, T. S., Campbell, J. W., 2011. Are the world's oceans optically different? J. Geophys. Res.,

15 116, C00H04, doi:10.1029/2011JC007230.

Teruzzi, A., Dobricic, S., Solidoro, C., Cossarini, G., 2014. A 3-D variational assimilation scheme in coupled transport-biogeochemical models: Forecast of Mediterranean biogeochemical properties, J. Geophys. Res. Oceans, 119, 200–217, doi:10.1002/ 2013JC009277.

Thuillier, G., Labs, D., Foujols, T., Peetermans, W., Gillotay, D., Simon, P. C., Mandel, H. 2003. The solar spectral

20 irradiance from 200 to 2400 nm as measured by the SOLSPEC spectrometer from the ATLAS and EURECA missions, 1–22.

Valente, A., Sathyendranath, S., Brotas, V., Groom, S., Grant, M., Taberner, M., Antoine,D., Arnone, R., Balch, W.M., Barker, K., Barlow, R., Bélanger, S., Berthon, J.F., Besiktepe, ¸S., Brando, V., Canuti, E., Chavez, F., Claustre, H., Crout, R., Frouin, R.,García-Soto, C., Gibb, S.W., Gould, R., Hooker, S., Kahru, M., Klein, H., Kratzer,S., Loisel, H., McKee, D., Mitchell, B.G., Moisan, T., Muller-Karger, F., O'Dowd, L.,Ondrusek, M., Poulton, A.J., Repecaud, M., Smyth, T., Sosik,

25 H.M., Twardowski, M.,Voss, K., Werdell, J., Wernand, M., Zibordi, G., 2016. A compilation of global bio-optical in situ data for ocean-colour satellite applications. Earth Syst. Sci. Data 8,235–252. http://www.earth-syst-sci-data.net/8/235/2016/. http://dx.doi.org/10.5194/essd-8-235-2016.

Volpe, G., Santoleri, R., Vellucci, V., Ribera d'Alcala, M., Marullo, S., D'Ortenzio, F., 2007. The colour of the Mediterranean Sea: Global versus regional bio-optical algorithms evaluation and implication for satellite chlorophyll

30 estimates, Remote Sens. Environ., 107, 625–638.

Volpe, G., Colella, S., Forneris, V., Tronconi, C., Santoleri, R., 2012. The Mediterranean Ocean Colour Observing System – system development and product validation. Ocean Sci., 8, 869–883.

Volpe, G., Buongiorno Nardelli, B., Colella, S., Pisano, A., Santoleri, R., 2018. An Operational Interpolated Ocean Colour Product in the Mediterranean Sea, in New Frontiers in Operational Oceanography, Ed. E.P. Chassignet, A. Pascual, J. Tintorè and J. Verron, in press.

von Schuckmann, K., Le Traon, P.-Y., Alvarez-Fanjul, E., Axell, L., Balmaseda, M., Breivik, L.-A., Verbrugge, N., 2017.
5   The Copernicus Marine Environment Monitoring Service Ocean State Report. Journal of Operational Oceanography, 9(sup2), s235–s320. http://doi.org/10.1080/1755876X.2016.1273446.

Zibordi, G., D'Alimonte, D., Berthon, J. F., 2004. An evaluation of depth resolution requirements for optical profiling in coastal waters. Journal of Atmospheric and Oceanic Technology, 21(7), 1059–1073. https://doi.org/10.1175/1520-0426(2004)021<1059:AEODRR>2.0.CO;2

10   Zibordi, G. and G. M. Ferrari, 1995. Instrument self-shading in underwater optical measurements: experimental data, Appl. Opt. 34, 2750-2754.

Zibordi, G., Hooker, S.B., Berthon, J.-F., D'Alimonte, D., 2002. Autonomous above-water radiance measurements from an offshore platform: a field assessment experiment. J. Atmos. Oceano. Tech., 19, 808-819.

Zibordi, G., Mélin, F., Berthon, J.F., Holben,   B., Slutsker, I., Giles, D., D'Alimonte, D., Vandemark, D., Feng, H.,
15   Schuster, G., Fabbri, B.E., 2009. AERONET-OC: a network for the validation of ocean color primary products. Journal of Atmospheric and Oceanic Technology, 26(8), pp.1634-1651.

Zibordi, G., Berthon, J.-F., Mélin, F., D'Alimonte, D., 2011. Cross-site consistent in situ measurements for satellite ocean color applications: the BiOMaP radiometric dataset, Rem. Sens. Environ., 115, 2104–2115.

Zibordi, G., Ruddick, K., Ansko, I., Moore, G., Kratzer, S., Icely, J., & Reinart, A. (2012). In situ determination of the
20   remote sensing reflectance: An inter-comparison. Ocean Science, 8(4), 567–586. https://doi.org/10.5194/os-8-567-2012.
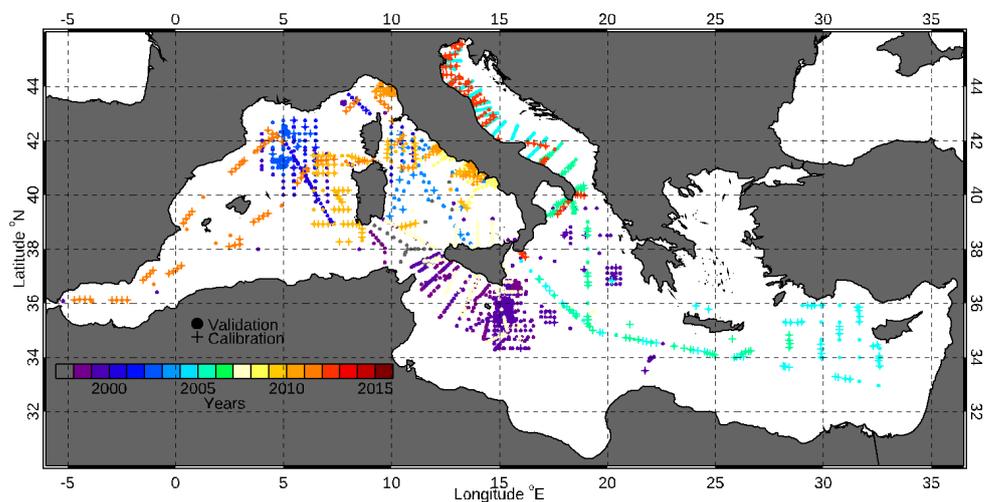
Figures

Figure 1: Study Area and space-time distribution of the in situ MedBiOp dataset (1997-2016) used in this work. Dots identify the in situ station used as sea-truth for satellite data validation, whereas crosses refer to the observations used to develop the regional OC algorithms.
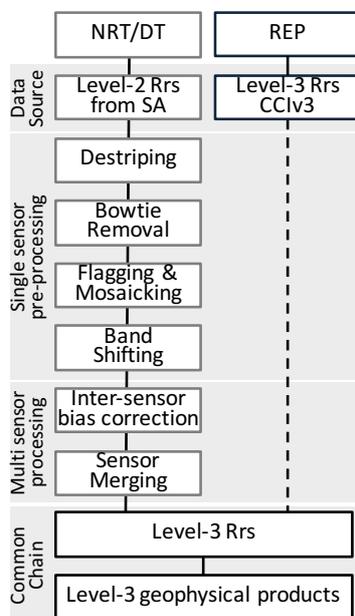
Figure 2: flowchart of the processing chains for the two data production lines, NRT/DT and REP modes. SA stands for space agencies. The dashed vertical line indicates that, the CNR REP processing mode only involves the application of the regional fine-tuned algorithms for the retrieval of the geophysical quantities.
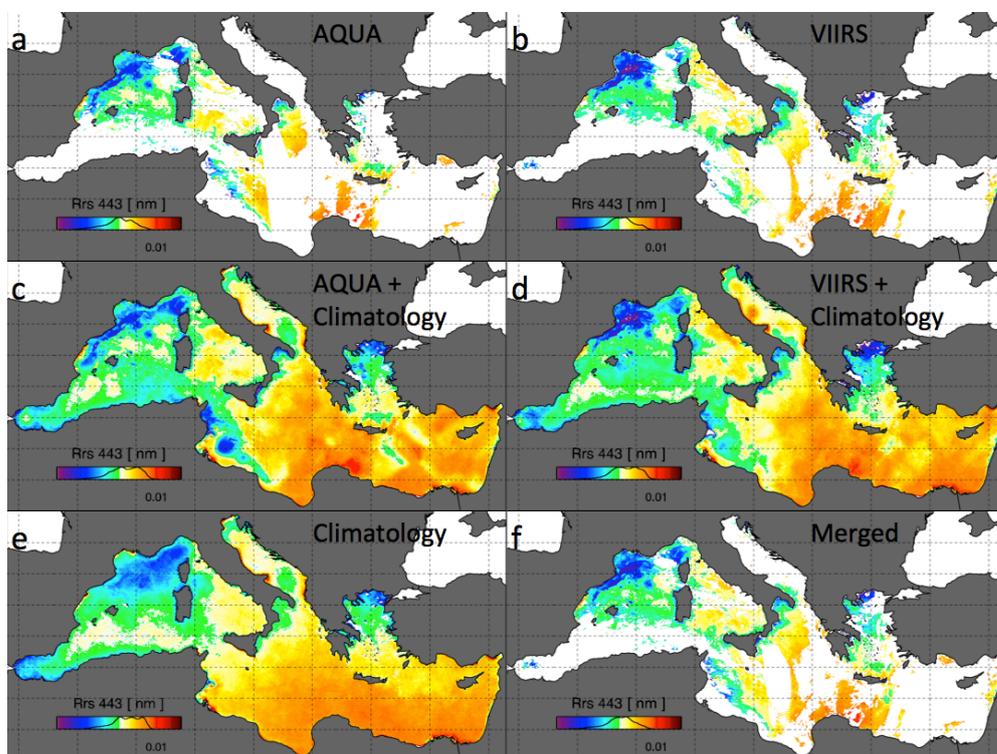
Figure 3: Example of how the merging of MODIS and VIIRS works. Rrs 443 from MODIS AQUA (a), NPP-VIIRS (b) from April 1st 2012. Panels c and d are obtained by filling in panels a and b with climatology (e). The merged multi sensor product is obtained after removal of the unseen pixels (f).
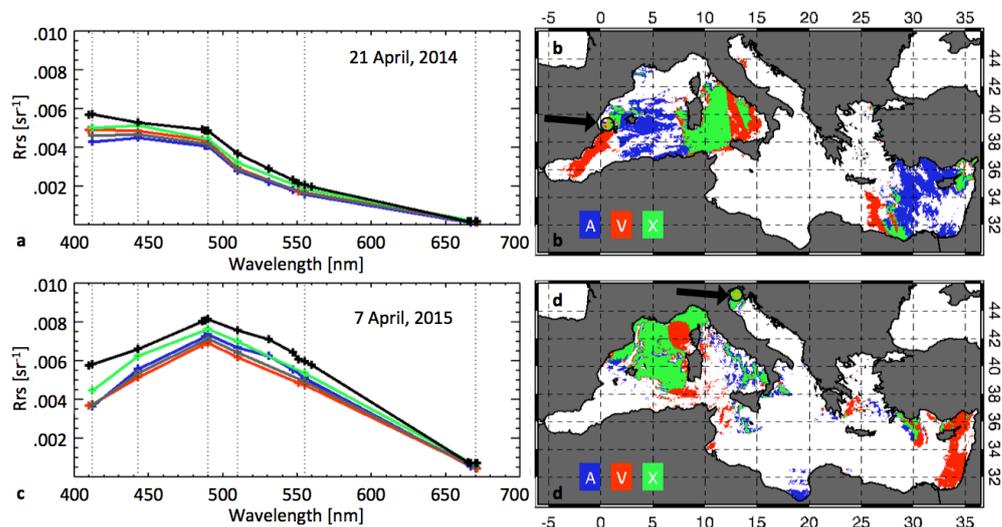
Figure 4: Rrs spectra from the 21st April, 2014 (panel a), from MODIS-AQUA (A, blue), NPP-VIIRS (V, red), the merged multi-sensor product with the application of the bias correction (X, green) and without (grey), and the in situ measurements (black), all in correspondence of the in situ measurement location shown by the arrow in panel b. The map in panel b is the sensor mask of the day in which the pixels sampled by MODIS-AQUA only are shown in blue and those by NPP-VIIRS only in red; the pixels sampled by both sensors are shown in green. Panel c and d refer to the Rrs spectra and sensor mask from the 7th April 2015, in the northern Adriatic Sea.
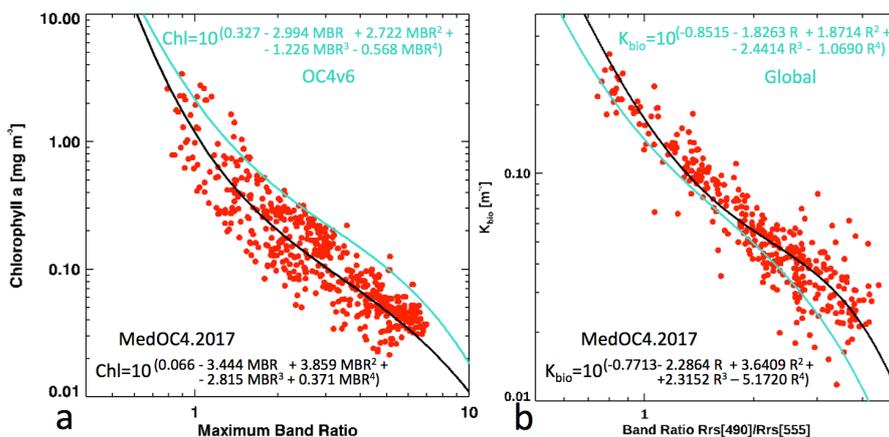
Figure 5: panel a: algorithm for chlorophyll retrieval over the Mediterranean Sea. The maximum band ratio (MBR) is shown on the X-axis; it is the ratio between the maximum value between the three bands in the blue (443, 490 and 510 nm) and the one in the green part of the light spectrum (555 nm). Red dots (N=509) are the in situ bio-optical data (whose location is shown in Figure 1) used to compute the operational algorithm (black line). As a means of comparison the global algorithm (OC4v6, https://oceancolor.gsfc.nasa.gov/atbd/chlor_a) functional form is also superimposed (turquoise line). Panel b: algorithm for the

retrieval of the diffuse attenuation coefficient, Kd490, over both the Mediterranean Sea (black line) and the global ocean (turquoise line). The global algorithm is the SeaWiFS (https://oceancolor.gsfc.nasa.gov/atbd/kd_490). Red dots (N=366) are the in situ measurements over the Mediterranean Sea. Differently than for Chl, here on the X-axis, the ratio between Rrs490 and Rrs555 is shown. Kd490 is the sum of Kbio and of the attenuation due to pure sea water (0.0166; Pope and Fry, 1972).
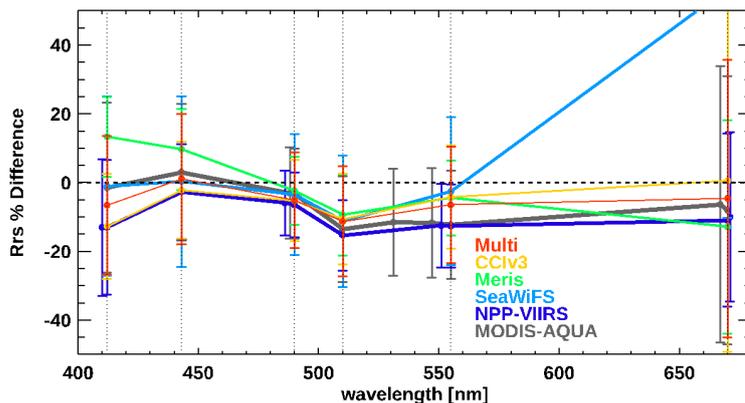
Figure 6: Relative difference between satellite and MedBiOp Rrs spectra for MODIS-Aqua (grey), NPP-VIIRS (blue), SeaWiFS (turquoise), MERIS (green), OC-CCI (yellow) and for the multi-sensor product developed and described in this work (red). Vertical bars represent one standard deviation from the average RPD value. Target wavelengths are marked with vertical dotted lines.
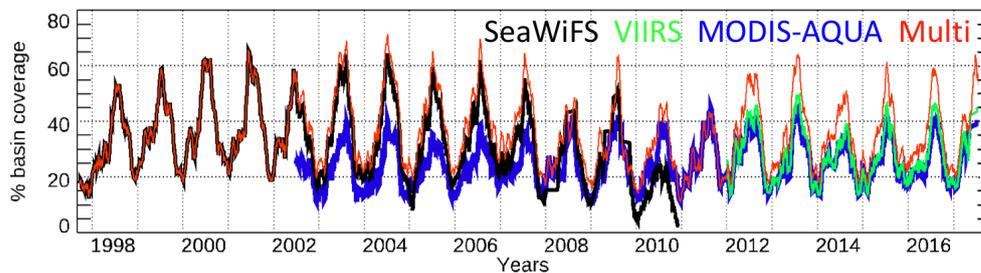
Figure 7: Time series of the number of pixels for each satellite sensor as percent with respect to the basin total coverage.
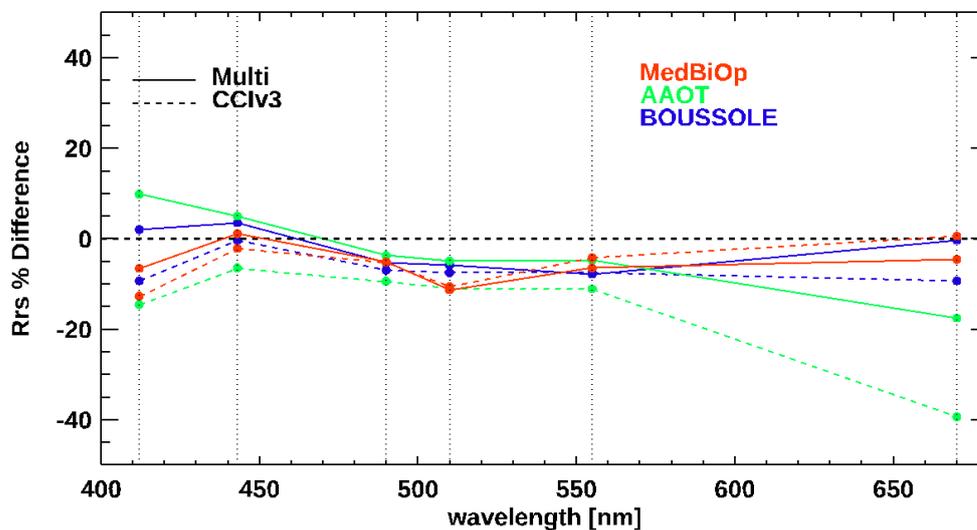
Figure 8: Relative difference between Multi and CCIv3 satellite observations and in situ measurements (MedBiOp in red, AAOT in green and BOUSSOLE in blue). The number of matchups used from each dataset is summarized in Table 3. Target wavelengths are marked with vertical dotted lines. As a reference the two red lines correspond to the red and orange lines in Figure 6.
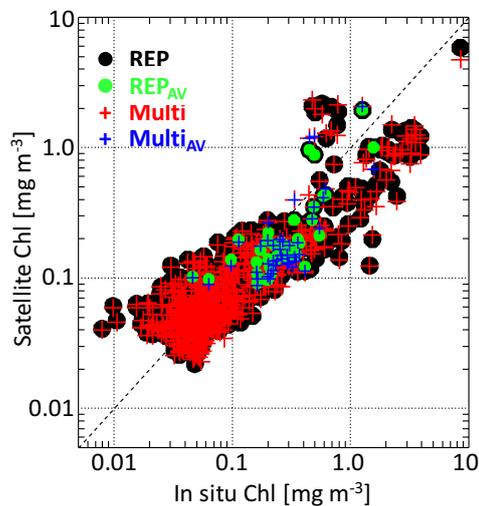
Figure 9: Satellite (y axis) versus in situ (MedBiOp) Chl concentration. Satellite Chl is the REP (derived by the application of the MedOC4.2017 to the Rrs derived from the CCIv3 processor, black) and NRT (derived from the Multi processing, red). Green dots

and blue crosses are the REP and NRT for matchups on the period in which VIIRS and MODIS co-exist (REP$_{AV}$ and Multi$_{AV}$). Statistics associated with the matchup comparison are shown in Table 4.

Tables

Wavelength (nm)	Sensors					REP	In situ
	VIIRS	MODIS	MERIS	OLCI	SeaWiFS		
410	•						
412		•			•	•	•
413			•	•			
443	•	•	•	•	•	•	•
486	•						
488		•					
490			•	•	•	•	•
510			•	•	•	•	•
531		•					
547		•					
551	•						
555					•	•	•
560			•	•			
665			•	•			•
667		•					
670					•	•	
671	•						

Table 1: Overview of the available wavelengths from VIIRS, MODIS, MERIS, OLCI and SeaWiFS sensors and those used to produce the REP dataset (available from PML) and those collected in situ. Target wavelengths of the band shifting procedure are highlighted in grey. Column "in situ" refers to the bands of the Lu, Ed and Es Satlantic radiometers used to compute the
10 **algorithm functional forms and described in the in situ data description section (The Mediterranean Sea in situ bio-optical dataset: MedBiOp).**

Name	Definition

Type-2 slope	$S = \dfrac{\sum\limits_{i=1}^{N}\left(X_i^E - \overline{X}^E\right)^2 - \sum\limits_{i=1}^{N}\left(X_i^M - \overline{X}^M\right)^2 + \left[\left\{\sum\limits_{i=1}^{N}\left(X_i^E - \overline{X}^E\right)^2 - \sum\limits_{i=1}^{N}\left(X_i^M - \overline{X}^M\right)^2\right\}^2 + 4\left\{\sum\limits_{k=k}^{N}\left(X_k^E - \overline{X}^E\right)\left(X_k^M - \overline{X}^M\right)\right\}^2\right]^{1/2}}{2\sum\limits_{i=k}^{N}\left(X_k^E - \overline{X}^E\right)\left(X_k^M - \overline{X}^M\right)}$
Type-2 intercept	$I = \overline{X}^E - S \cdot \overline{X}^M$
Determination coefficient	$r^2 = \dfrac{\left[\sum\limits_{i=1}^{N}\left(X_i^E - \overline{X}_i^E\right)\left(X_i^M - \overline{X}_i^M\right)\right]^2}{\sum\limits_{i=1}^{N}\left(X_i^E - \overline{X}_i^E\right)^2 \sum\limits_{i=1}^{N}\left(X_i^M - \overline{X}_i^M\right)^2}$
Root Mean Square Difference	$RMSD = \sqrt{\dfrac{\sum_{i=1}^{N}(X_i^E - X_i^M)^2}{N}}$
Bias	$bias = \dfrac{1}{N}\sum\limits_{i=1}^{N}(X_i^E - X_i^M)$
Relative percentage Difference	$RPD = 100 \cdot \dfrac{1}{N}\sum\limits_{i=1}^{N}\dfrac{X_i^E - X_i^M}{X_i^M}$
Absolute percentage Difference	$APD = 100 \cdot \dfrac{1}{N}\sum\limits_{i=1}^{N}\dfrac{\left|X_i^E - X_i^M\right|}{X_i^M}$

Table 2: Metrics used to compare the estimated (satellite-based) dataset X^E to a reference, measured in-situ dataset X^M. A more comprehensive table of metrics is provided in Supplementary Material (Table S.1).

Rrs	Slope	Intercept	r^2	RMSD	Bias	RPD	APD	N
412	0.99	-0.0006	0.78	0.0015	-0.00060	-7	17	272
443	0.85	0.0007	0.73	0.0013	-0.00022	1	15	272
490	0.66	0.0015	0.55	0.0013	-0.00047	-5	13	272
510	0.65	0.0009	0.57	0.0013	-0.00059	-11	18	272
555	0.68	0.0005	0.71	0.0012	-0.00027	-6	16	272
670	1.19	-0.0001	0.91	0.0002	-0.00001	-1	35	194

Table 3: Statistics associated with the Multi Rrs product computed over the MedBiOp dataset. The same statistics associated with
5 all products shown in Figure 6 are provided in Supplementary Material (Table S.2 to Table S.7).

Bands [nm]

in situ	Satellite	412	443	490	510	555	670
MedBiOp	Multi	265	265	265	265	265	192
	CCIv3	255	255	255	255	255	219
AAOT	Multi	1510	1510	1510	1510	1510	1027
	CCIv3	1726	1726	1726	1726	1726	1477
BOUSSOLE	Multi	754	754	754	754	754	582
	CCIv3	882	882	882	882	882	780

Table 4: Number of matchups used to compute the statistics presented in Figure 8.

Product	Slope	Intercept	r^2	RMSD	Bias	RPD	APD	N
REP	0.737	-0.306	0.75	0.253	-0.043	7	47	708
Multi	0.752	-0.308	0.74	0.259	-0.060	3	47	708
REP_{AV}	1.052	-0.108	0.57	0.242	-0.138	-18	43	44
$Multi_{AV}$	1.183	-0.047	0.50	0.273	-0.151	-17	48	44

Table 5: Statistics about the three Chl matchup datasets described in Figure 9. The first two rows refer to the comparison of the two satellite multi-sensor products with the entire MedBiOp Chl dataset, while the last two refer to the statistics associated with matchups on the period in which VIIRS and MODIS co-exist (REP_{AV} and $Multi_{AV}$). A more comprehensive table of metrics is provided in Supplementary Material (Table S.8).